Frontiers of Physics
https://doi.org/10.1007/s11467-021-1067-8
Front. Phys.
16(5), 53503 (2021)

RESEARCH ARTICLE

$BiVO_4/TiO_2$ heterojunction with rich oxygen vacancies for enhanced electrocatalytic nitrogen reduction reaction

Yunliang Liu[1], Peiji Deng[1,6], Ruqiang Wu[1], Ramadan A. Geioushy[2], Yaxi Li[1], Yixian Liu[1,†], Fengling Zhou[3,‡], Haitao Li[1,4,#], Chenghua Sun[5,§]

[1] *Institute for Energy Research, School of Chemistry and Chemical Engineering, Jiangsu University, Zhenjiang 212013, China*
[2] *Nanomaterials and Nanotechnology Department, Advanced Materials Division, Central Metallurgical R&D Institute (CMRDI), P.O. Box, 87 Helwan, 11421, Cairo, Egypt*
[3] *College of Chemical Engineering and Energy Technology, Dongguan University of Technology, Dongguan 523808, China*
[4] *Guangxi Key Laboratory of Electrochemical Energy Materials, Guangxi University, Nanning 530004, China*
[5] *Faculty of Science, Engineering & Technology, Swinburne University of Technology, Victoria 3122, Australia*
[6] *Faculty of Engineering, The University of Sydney, Sydney, Australia*
Corresponding authors. E-mail: [†] *lucien_xian@163.com,* [‡] *zhoufl@dgut.edu.cn,* [#] *liht@ujs.edu.cn,* [§] *Chenghuasun@swin.edu.au*
Received November 26, 2020; accepted March 5, 2021

The large-scale production of ammonia mainly depends on the Haber–Bosch process, which will lead to the problems of high energy consumption and carbon dioxide emission. Electrochemical nitrogen fixation is considered to be an environmental friendly and sustainable process, but its efficiency largely depends on the activity and stability of the catalyst. Therefore, it is imperative to develop high-efficient electrocatalysts in the field of nitrogen reduction reaction (NRR). In this paper, we developed a $BiVO_4/TiO_2$ nanotube ($BiVO_4$/TNT) heterojunction composite with rich oxygen vacancies as an electrocatalytic NRR catalyst. The heterojunction interface and oxygen vacancy of $BiVO_4$/TNT can be the active site of N_2 dynamic activation and proton transition. The synergistic effect of TiO_2 and $BiVO_4$ shortens the proton transport path and reduces the over potential of chemical reaction. $BiVO_4$/TNT has high ammonia yield of 8.54 $\mu g \cdot h^{-1} \cdot cm^{-2}$ and high Faraday efficiency of 7.70% in −0.8 V vs. RHE in 0.1 M Na_2SO_4 solution.

Keywords TiO_2 nanotubes, $BiVO_4$, interface, oxygen vacancy, NRR

1 Introduction

Nitrogen is an important component of the basic units of protein, enzyme, nucleic acid, and so on [1–3]. Although nitrogen accounts for about 78% of air, because of its strong ties, electronegativity and ionization characteristics, such natural resource cannot be used directly by most of the organisms, so a sustainable development route to obtain fixed nitrogen compounds like ammonia is necessary to serve human society from development of agricultural fertilizer to safety of energy storage [4, 5]. In the industrial field, a large scale of ammonia synthesis is achieved by Haber–Bosch process. This process needs to burn a large number of fossil fuels to supply heat energy and emits a large amount of carbon dioxide, which intensifies the greenhouse effect of the earth [6–9]. Therefore, it is urgent to develop a new route of ammonia synthesis under mild conditions for energy conservation and environmental protection [10–13]. Electrocatalytic nitrogen reduction can theoretically be carried out at room temperature and atmospheric pressure, and the raw materials (water and nitrogen) are widely sourced in nature, which brings an opportunity to achieve the green synthesis of ammonia under mild conditions [14–16]. However, due to the difficulty of activation and fracture of N≡N triple bond and the low solubility of nitrogen, the electro-reduction of nitrogen is very difficult to be carried out in thermodynamics and kinetics [17–20]. Moreover, the existence of hydrogen evolution competition reaction will consume part of electrons and further lead to lower efficiency and selectivity of electrocatalytic nitrogen reduction reaction (NRR). Therefore, how to improve the selectivity of electrocatalytic NRR and then improve the efficiency of ammonia synthesis is a major challenge for the electrochemical synthesis of ammonia at room temperature and atmospheric pressure [21–23].

Generally, the catalyst is the key factor for the efficient electrocatalytic NRR under ambient conditions. Heterojunction and defect engineering located at heterogeneous

*Special Topic: Heterojunction and Its Applications (Ed. Chenghua Sun). This article can also be found at http://journal.hep.com.cn/fop/EN/10.1007/s11467-021-1067-8.

© Higher Education Press 2021

structure interfaces are often considered active sites that promote charge separation and electron transfer during reactions. Noble-metal catalysts (Au, Pd, Rh and Ru) [24–27] demonstrate favorable catalytic activities on NRR, but limited resources and high cost hinder large-scale industrialization. Nowadays, metal oxides are receiving increasing attention as promising alternative NRR catalysts due to their availability and respectable catalytic activities. Metal oxide interface plays an important role in improving catalytic activity due to the strong interface interaction. It can improve the stability of active sites for molecular activation [28]. It has been verified in carbon dioxide reduction [29, 30], methanol oxidation [31, 32], and ammonia synthesis [33]. Meanwhile, oxygen atoms on the surface of oxide catalysts are dug and squeezed by various physical and chemical methods to forming OVs with a positive charge, so as the electrons captured by the OVs can be injected into the anti-bonding orbit of N_2, which weakens the N≡N triple bond, reduces the reaction energy barrier and restrains the hydrogen evolution reaction. Therefore, the performance of NRR can be improved by the injection of OVs [34–36]. It is a good strategy to design a composite material with heterojunction interface effect and vacancy effect. The valence states of TiO_2 transition elements are +4. With the change of external conditions, they are easy to form low valence state, such as Ti^{3+}, thus exposing OVs [37, 38]. In recent years, TiO_2, as the most common semiconductor material, has been widely used in energy-related research. TiO_2 [39–45] has been reported that it has a good performance in electrocatalytic nitrogen fixation, however, due to the weakness of its conductivity and ability to transmit electric charge, it needs to be doped or modified to reverse these disadvantages. On the other hand, the atomic number of Bi in the periodic table of elements is 83, Bi-related semiconductor materials express the advantages of good conductivity, low price and innocuity. Due to the higher adsorption free energy base between Bi and H_2, Bi is a material with low activity of hydrogen evolution reaction. Bi 6p band and N 2p orbit of interaction between N_2 selective adsorption on the surface could help for N ≡ N dissociation, so Bi or Bi-based material should be material has superior performance in electrocatalysis nitrogen fixation [46, 47]. As a Bi-based semiconductor material, $BiVO_4$ can easily form defective oxygen vacancies on the surface, and its low-coordination V atoms are spin-polarized, which helps the activation and cleavage of N_2 molecules.

Therefore, we synthesized a $BiVO_4$/TNT heterojunction composite with oxygen vacancy and applied it for N_2 fixation. Firstly, a two-step electrochemical method is used to synthesize TiO_2 nanotubes on Ti foil. Then $BiVO_4$ is loaded on the TiO_2 nanotubes by hydrothermal method. TiO_2 nanotubes provide more reaction attachment sits concentrated on OVs, while $BiVO_4$ [48, 49] optimizes the conductivity of composite and promotes electron transport. so that the catalytic performance of the composite is expected to be improved. $BiVO_4$ is supported on the surface of TNT to form a heterojunction with a synergistic effect between these two components [33], which retains the respective properties.

In this paper, we use electrochemical oxidation method to synthesize TiO_2 nanotubes with a very uniform tubular structure. Through the hydrothermal method, $BiVO_4$ is loaded on TiO_2 nanotubes, and the composite as electrode has relatively high efficiency and stable electrocatalytic nitrogen fixation performance. The electrochemical test shows that $BiVO_4$/TNT have higher ammonia yield of 8.54 $\mu g \cdot h^{-1} \cdot cm^{-2}$ and higher Faraday efficiency (FE) of 7.70% in –0.8 V vs. RHE in 0.1 M Na_2SO_4 solution.

2 Experiment

2.1 TiO_2 nanotube preparation

2.5 cm ×1.5 cm titanium foil was cleaned by acetone, ethanol and water separately. Then the Ti foil was dried with nitrogen and further anodized in the solution of 98 mL glycol, 0.33 g NH_4F and 2 mL deionized water for the first time. The graphite plate was used as the opposite electrode. The reaction was under 60 V for 4 hours. Then the Ti foil was took out and washed by water and ethanol, and further dried in the air. The TiO_2 film can be removed by ultrasonic method. The remaining Ti foil was

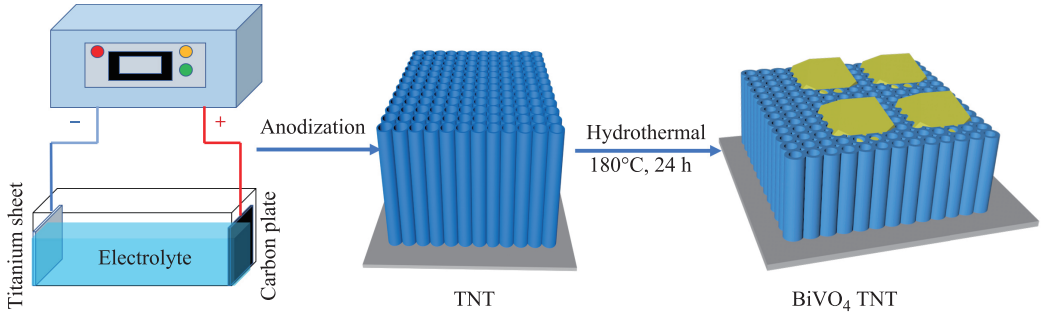


Fig. 1 Schematic route for the synthesis of $BiVO_4$/TNT heterojunction.

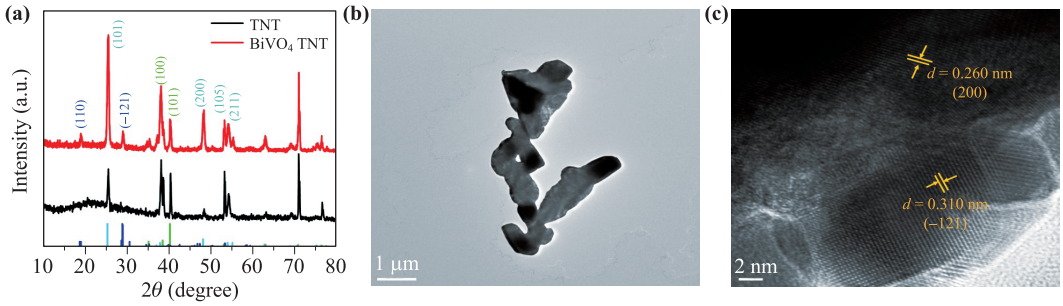


Fig. 2 Experimental characterization. **(a)** XRD patterns of $BiVO_4$ and $BiVO_4$/TNT; **(b)** TEM image of $BiVO_4$ and **(c)** HRTEM image of $BiVO_4$.

anodized for the second time, under 50 V. After oxidized in the electrolyte for 1.5 h, high-quality TiO_2 nanotubes were obtained on the Ti foil substrate (called TNT).

2.2 $BiVO_4$/TNT preparation

Firstly, 0.03 M $BiNO_3{\cdot}5H_2O$ was dissolved in 30 mL 1 M nitric acid solution (solution 1), 0.05 M NH_4VO_3 was dissolved in 30 mL 1 M NaOH solution (solution 2). Then solution 2 was added into solution 1 drop by drop; secondly, TNT was placed on the bottom of 100 mL Teflon-lined stainless-steel autoclave, and the obtained mixed solution was transformed to the autoclave. The reaction conducted at 180°C for 24 h. After cooling down to room temperature, the product was washed with ethanol and water, and then dried to obtain $BiVO_4$/TNT. The scheme of synthesis procedure is shown in Fig. 1.

3 Characterization

X-ray diffraction (XRD) patterns of the prepared TNT and $BiVO_4$/TNT are shown in Fig. 2(a). For the XRD of TNT, the main peak angles at 25.28, 48.05, 53.89 and 55.06 respectively correspond to (101), (200), (105) and (211) crystal faces of TiO_2 (JCPDS Card No.21-1272), while the main peak angles at 35.09, 38.42 and 40.17 respectively correspond to (100), (002) and (101) of Ti (JCPDS Card No.44-1294). Compared with pure TNT, $BiVO_4$/TNT has two smaller peaks at diffraction angles of 18.67 and 28.82, which correspond to (110) and (−121) of $BiVO_4$ (JCPDS Card No.14-0688). It indirectly proves that $BiVO_4$ was loaded on TNT successfully. The morphologies and structures of the obtained $BiVO_4$ and $BiVO_4$/TNT were characterized by TEM and SEM Figs. 2(b) and (c) are the $BiVO_4$ TEM and HRTEM images. From Fig. 2(b), it can be seen that the pure $BiVO_4$ has a block structure with a length between 1–2 μm. Figure 2(c) shows that the two different lattices spacing of $BiVO_4$ are 0.26 nm and 0.31 nm, respectively, which correspond to its crystal planes of (200) and (−121). Figures 3(a) and (b) show the SEM images of TNT. Figure 3(a) indicates that the TNT has a very uniform tubular structure with small holes which their diameters

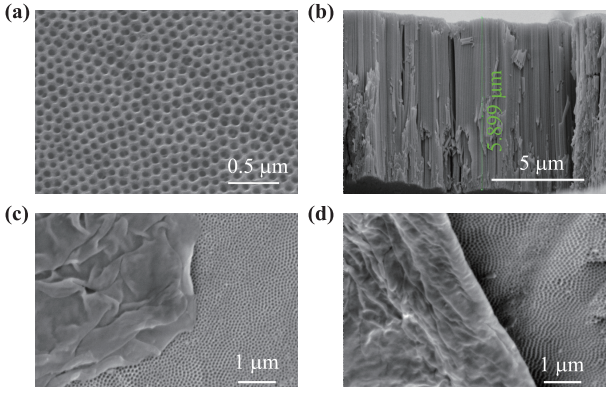


Fig. 3 **(a, b)** SEM images of TNT; **(c, d)** SEM images of $BiVO_4$/TNT.

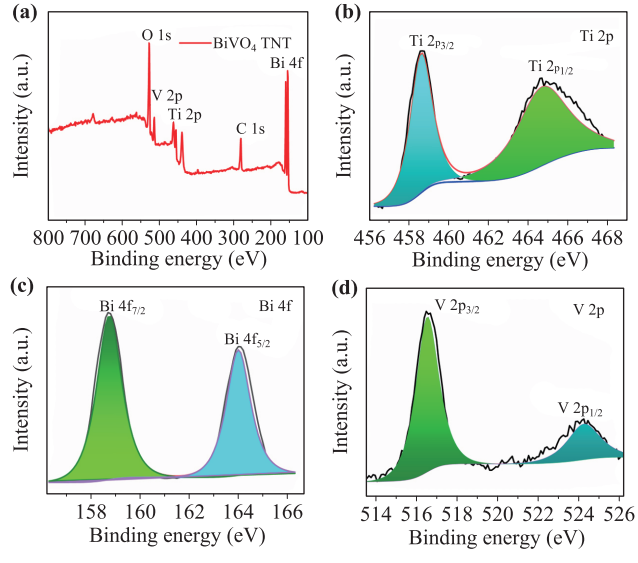


Fig. 4 XPS spectra of $BiVO_4$/TNT: **(a)** Survery; **(b)** Ti 2p; **(c)** Bi 4f; **(d)** V 2p.

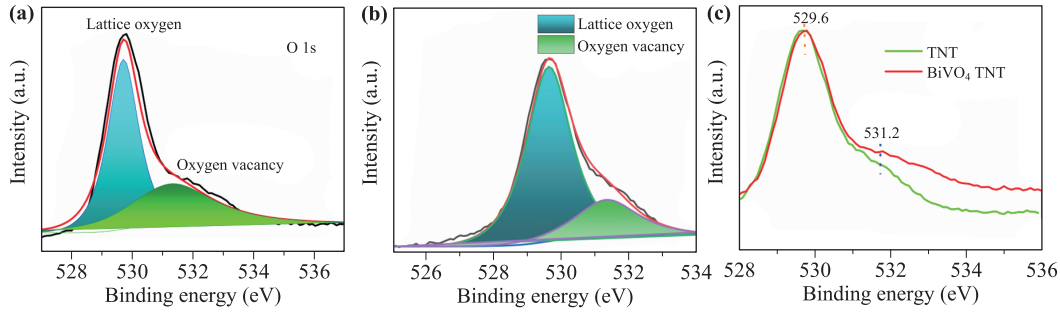


Fig. 5 O1s of TNT **(a)** and $BiVO_4$/TNT **(b)**; **(c)** O1s normalization comparison of TNT and $BiVO_4$/TNT.

are about 100 nm. Figure 3(b) is the cross-section view of TNT, which confirms that the length of nanotubes is around 5 μm. Figure 3(c) indicates flake-like $BiVO_4$ loaded on TNT surface while Fig. 3(d) reveals the topography of the joint of $BiVO_4$ and TNT, and further formed a connection structure.

In order to investigate the elemental constitutes and oxidation states of the composite, X-ray photoelectron spectroscopy (XPS) was applied to analyze the $BiVO_4$/TNT sample. Figure 4(a) shows the full XPS peaks of $BiVO_4$/TNT, including the elements of Bi, V, O and Ti. Figure 4(b) spreads the diffraction peak of Ti 2p, with the peak positions of 458.4 eV and 465.2 eV. Figure 4(c) shows the diffraction peak of Bi 4f, with the peak positions of 158.6 eV and 164.0 eV. Figure 4(d) reveals the diffraction peak of V 2p, with the peak positions of 516.6 eV and 524.1 eV. Figure S1 shows the XPS of TNT, including the elements of O and Ti. The O 1s peaks of $BiVO_4$/TNT and TNT are shown in Figs. 5(a) and (b), where 529.6 eV represents lattice oxygen and 531.2 eV stands for oxygen vacancies. After normalized the O 1s peaks, it can be seen from Fig. 5(c) that $BiVO_4$/TNT has more oxygen vacancies than the pure TNT, thus meaning that the composite can provide more active sites for the reaction.

4 Electrochemical performance test

The electrocatalytic properties of NRR were studied systematically in 0.10 M Na_2SO_4 by the aqueous solution of air tight H-cell. The anode chamber and cathode chamber containing 30 mL electrolyte solution were separated by Nafion 117 membrane. Then, $BiVO_4$/TNT was used as the working electrode of electrocatalytic NRR. Nitrogen gas (99.999%) was firstly bubbled into the cathode chamber for 30 min (50 mL·min^{-1}) Then, the bubbling rate was changed into a constant flow rate of 20 mL·min^{-1} during the whole electrolysis process, as shown in Fig. S2. During the whole measurement process, magnetic stirring maintained 400 rpm/min in the cathode chamber. Two glass vials containing 5 mL 0.05 M H_2SO_4 were used to connect with the cathode chamber to trap the escaped ammonia and prevent the contamination from the air, respectively.

The potential dependence of electrocatalytic NRR activity of the $BiVO_4$/TNT was investigated firstly. As shown in Fig. 6(a), the linear sweep voltammograms (LSV) curves of the catalyst in 0.10 M Na_2SO_4 electrolyte Ar-saturated or N_2-saturated 0.10 M Na_2SO_4 electrolyte are measured successively with the same working electrode. Under the condition of Ar and N_2 saturation, the cathode current begins to appear at about −0.6 V vs. RHE, while the higher current density can be clearly seen in the N_2 saturated electrolyte, indicating the additional contribution of NRR and the $BiVO_4$/TNT possesses catalytic activity for the NRR. According to the polarization curve and deflection potential, the suitable potential window range of electrocatalytic NRR is −0.6 V to −1.0 V vs. RHE. After electrolysis for 2 hours at a specific potential of −0.6 V to −1.0 V vs. RHE, the generated NH_3 was quantitatively determined by indophenol blue method.

Figure 6(b) shows the *i*–*t* curves of electrode decorated

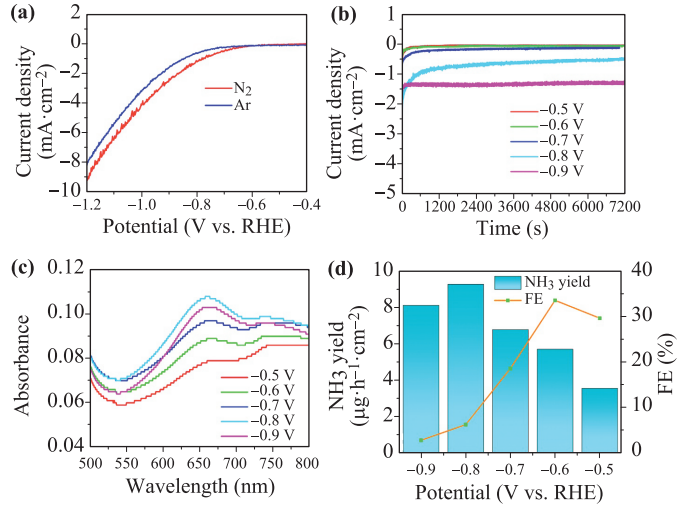


Fig. 6 **(a)** LSV curves of $BiVO_4$/TNT in Ar- and N_2-saturated solutions; **(b)** *i*–*t* curves under different potentials; **(c)** the UV-Vis spectra of the electrolyte under different potentials in N_2-saturated after the reaction; **(d)** NH_3 yields and FEs of $BiVO_4$/TNT under different potentials in N_2-saturated solution. All the tests are performed in 0.1 M Na_2SO_4 solution under ambient conditions.

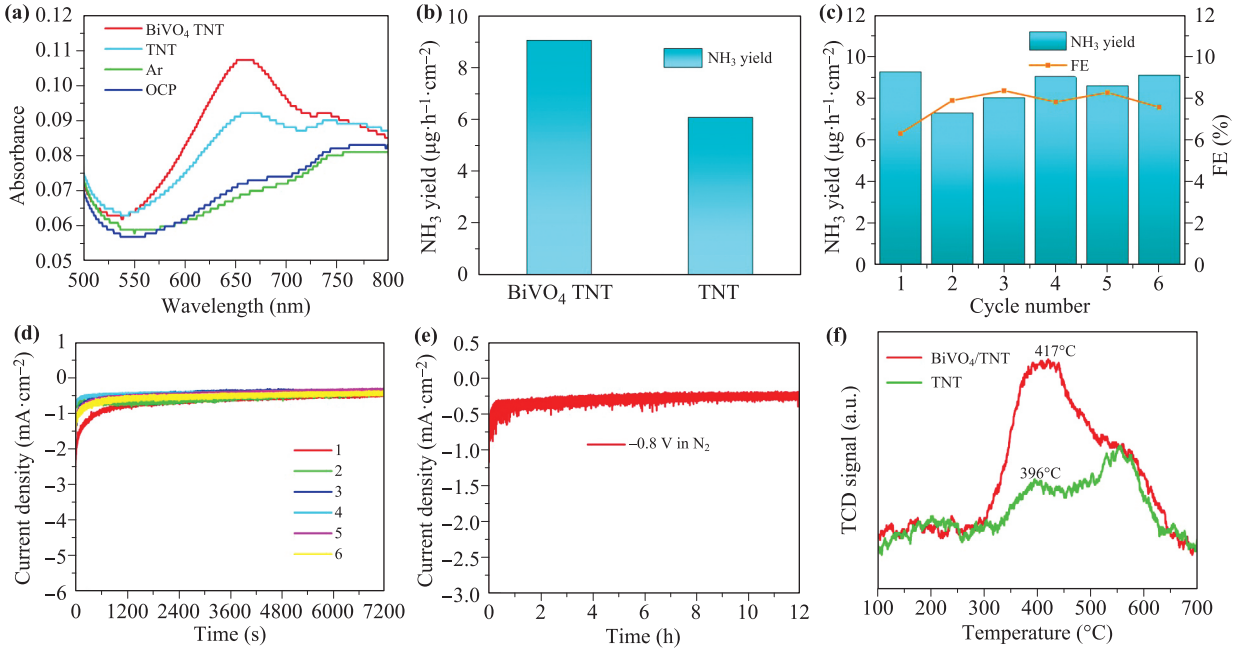


Fig. 7 **(a)** UV-Vis spectra of in $BiVO_4$/TNT saturated in N_2-/Ar-saturated solutions, N_2-saturated solution at open circuit, and N_2-saturated solution on pristine TNT; **(b)** NH_3 yields of TNT and $BiVO_4$/TNT at −0.8 V vs. RHE for 6 cycles; **(c)** NH_3 yields and FEs of $BiVO_4$/TNT at −0.8 V vs. RHE for 6 cycles; **(d)** *i*–*t* curves of $BiVO_4$/TNT at −0.8 V vs. RHE for 6 cycles. **(e)** long-term *i*–*t* curves of $BiVO_4$/TNT electrode showing good stability. **(f)** N_2 temperature-programmed desorption (N_2-TPD) curves of TNT and $BiVO_4$/TNT.

$BiVO_4$/TNT at different applied potentials, the steady current density in NRR test explains that the catalyst has good chemical stability. The output of ammonia was studied by UV-Vis absorption spectrum of the electrolyte for 2 hours with indophenol blue indicator method. Figure 6(c) shows the UV absorption curve under different potentials, and the highest absorption intensity, which means the highest ammonia generation rate, was obtained under –0.8 V vs. RHE. Furthermore, Fig. 6(d) shows the NH_3 yields and FEs of $BiVO_4$/TNT under different potentials in N_2-saturated solution. According to the UV absorption peak at 655 nm, the ammonia production rate under different applied potentials was calculated by comparing the measured ammonia standard curve (Figs. S1 and S2). The $BiVO_4$/TNT composite has the highest ammonia production rate of 8.54 $\mu g \cdot h^{-1} \cdot cm^{-2}$ and higher FE (7.70%) under –0.8 V vs. RHE. It is worth noting that, with a more negative potential applied, the NH_3 yield and FE were significantly reduced (–0.9 V vs. RHE). The reason is estimated that the effective adsorption sites of nitrogen are hindered by more protons. $BiVO_4$/TNT has good selectivity in the electrocatalytic synthesis of ammonia. It can be proven according to Fig. S3 where is almost no hydrazine formation.

In order to verify that the source of ammonia is nitrogen rather than other possible nitrogen-containing substances, we conducted a series of control experiments to detect the ammonia yields, including air potential measurement (open circuit potential, OCP) under nitrogen flow, TNT measurement under nitrogen flow and $BiVO_4$/TNT measurement under argon at –0.8 V vs. RHE. According to the UV absorption results, as shown in Fig. 7(a), there are almost no obvious peaks under OCP and Ar conditions. The production of ammonia indirectly proves that the source of nitrogen is nitrogen gas. On the other hand, the peak value of electrocatalytic nitrogen fixation of TNT is significantly lower than that of $BiVO_4$/TNT, which further implies that the electrocatalytic nitrogen fixation performance of $BiVO_4$/TNT is better than that of TNT. In Fig. 7(b), it is obvious that the ammonia yield of $BiVO_4$/TNT is higher than that of pure TNT. In order to evaluate the stability of the catalyst, we repeated NRR tests six times under –0.8 V vs. RHE, as shown in Fig. 7(c). It can be seen that the ammonia production rate and FE are almost unchanged after 6 times tests. The ammonia yield is always around 8.5 $\mu g \cdot h^{-1} \cdot cm^{-2}$ and the FE is around 8%. For the *i*–*t* curve during the tests [Fig. 7(d)], the current densities were almost in a constant straight line, and the cycle current was almost unchanged. Notably, Fig. 7(e) indicates that the *i*–*t* curve nearly kept the same current within 12 h reaction, which further highlighted the stability of the $BiVO_4$/TNT catalyst. In addition, in Fig. 7(f), the N_2-TPD curves show that the undoped TNT and $BiVO_4$/TNT displays two obvious different chemisorption peaks within the range of 100–700°C, which could be due to the different N_2 adsorption strength

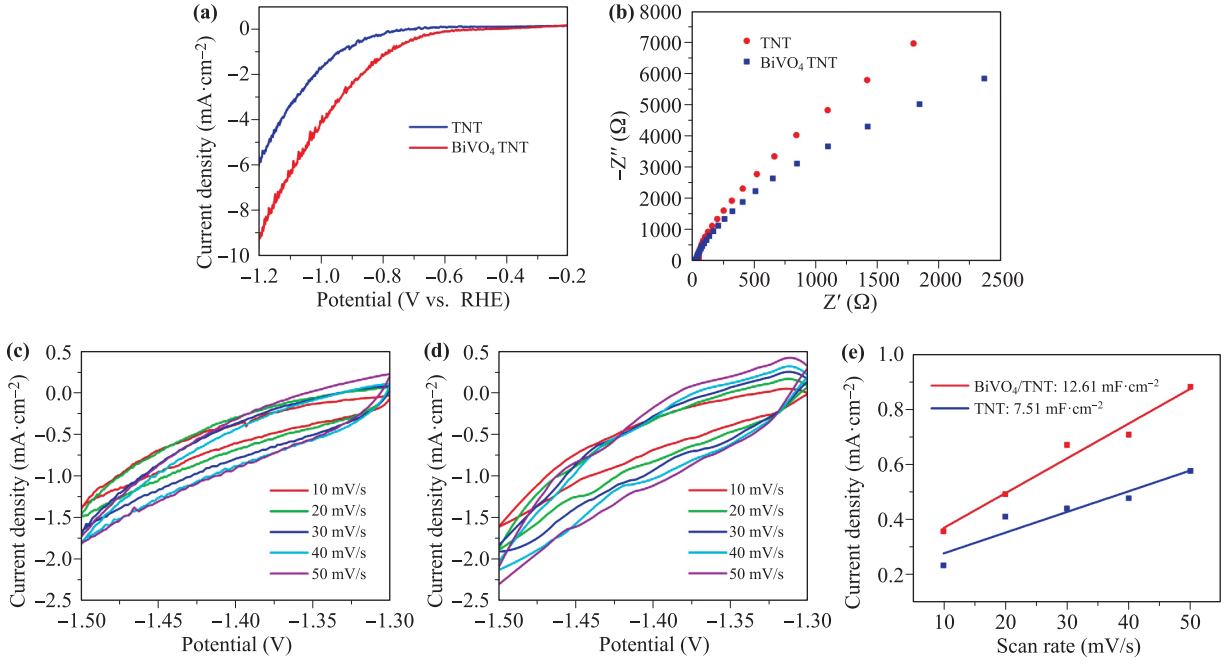


Fig. 8 **(a)** LSV of TNT and $BiVO_4$/TNT; **(b)** Electrochemical impedance spectra of TNT and $BiVO_4$/TNT, CV of **(c)** TNT and **(d)** $BiVO_4$/TNT at various scan rates from 10 to 50 $mV{\cdot}s^{-1}$) in the region of −1.5 V to −1.3 V vs. Ag/AgCl; **(e)** The capacitive current densities at −1.4 V vs. Ag/AgCl as a function of scan rates for TNT and $BiVO_4$/TNT.

on the surface of the catalysts. The chemisorption peaks of $BiVO_4$/TNT at 417°C are higher than that of TNT (396°C), which indicates that $BiVO_4$/TNT heterostructure can effectively improve the chemisorption of N_2 and subsequently makes the NRR performance.

In order to initially detect the catalyst's activity of NRR, we also measured the LSV curves of TNT and $BiVO_4$/TNT in N_2-saturated electrolyte with a rotation rate of 600 rpm and a scanning rate of 5.0 $mV{\cdot}s^{-1}$, as shown in Fig. 8(a). It can be seen that the current value of $BiVO_4$/TNT is higher than that of TNT at the same potential, which visibly confirms that the catalytic activity of $BiVO_4$/TNT is higher than the pure TNT. Figure 8(b) shows the impedance diagram of TNT and $BiVO_4$/TNT. Accordingly, a smaller impedance radius of $BiVO_4$/TNT means the smaller resistance value of $BiVO_4$/TNT than that of pure TNT, further confirming that the composite offers better performance for the electron transfer from the electrode to the decorated catalyst surface or interface. Figures 8(c) and (d) show the CV plots of $BiVO_4$/TNT and TNT at different scanning speeds from 10 mV/s to 50 mV/s, and the scanning area of $BiVO_4$/TNT is larger with the increasing of scanning rate. Figure 8(e) shows Tafel slopes of $BiVO_4$/TNT and TNT, in which $BiVO_4$/TNT presents a slope of 12.61 $mF{\cdot}cm^{-2}$, being slightly higher than that of TNT (7.51 $mF{\cdot}cm^{-2}$), which further supports that $BiVO_4$/TNT composite is more suitable for NRR. Based on the above analysis and the steps of nitrogen reduction summarized by predecessors [50], a possible NRR mechanism of $BiVO_4$/TNT has been proposed in Fig. 9: (i) TNT, due to its porous structure, can strongly combine with $BiVO_4$, to form $BiVO_4$/TNT heterojunction; (ii) oxygen vacancies in $BiVO_4$/TNT promote N_2 adsorption and reduction when protons have been co-adsorbed; and (iii) continuous adsorption of H protons from the electrolyte can attack and destroy the N≡N bond, resulting the final formation of ammonia. Clearly, porous TNT serves as the substrate to host $BiVO_4$ and active site to provide H-sources for NRR over the interface, and $BiVO_4$ can fix N_2 and boost its reduction.

To study the reasons promoting the nitrogen fixation on

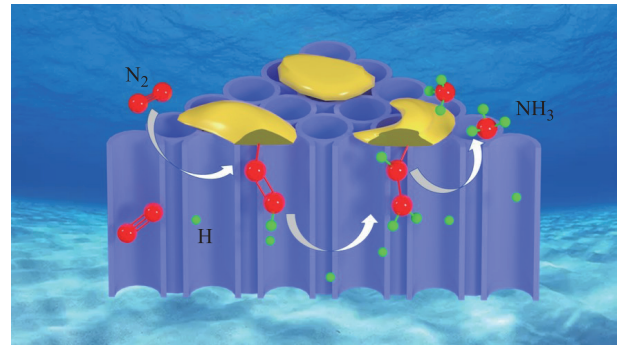


Fig. 9 The pathway for electrochemical NRR on $BiVO_4$/TNT interface under ambient condition.

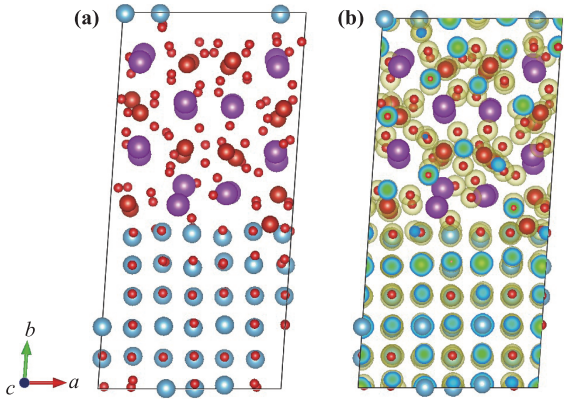


Fig. 10 **(a)** The crystal structure of heterojunction and **(b)** its charge distribution. The electron density on yellow isosurface is 0.2 e/Bohr^3.

the interface of $BiVO_4$/TNT from the view of electronic structure, a first-principles calculation is carried out (the detailed calculation settings are introduced in supporting information). The relaxed interface structure (heterojunction) is shown in Fig. 10(a) and the charge distribution of heterojunction is shown in Fig. 10(b) in order to provide a straightforward observation of the electronic structure.

To make a detailed analysis on the electronic structure of $BiVO_4/TiO_2$ interface, the Bader analysis is adopted to calculate the charge (or "captured" electrons) of each atom. It is found that, for the same element, the charge of each atom in $BiVO_4/TiO_2$ heterojunction distribute on a wide range rather than varying slightly along with a certain value. To make this clear, the charge of atoms in single phase and heterojunction are plotted in the same histogram. Considering that both $BiVO_4$ and TiO_2 contain element O, two histograms of O charge are plotted. The histograms are shown in Fig. 11. It is notable that, although all the atoms in involved cells are counted, the different size between cells results in different number of counted atoms in histogram, which, however, does not influence our analysis since only the tendency of charge transfer is concerned.

According to Figs. 11(a) and (b), it can be deduced that the charge of O in TiO_2 does not change much after becoming a heterojunction, but there is an obvious electron loss for O atoms in $BiVO_4$. In contrast, as shown in Figs. 11(c)–(e), the metal elements Ti, Bi and V obtain some electrons after forming heterojunctions. Considering that the structures of $BiVO_4$ and TiO_2 are incoherent, there are massive defects along with their interface in heterojunction, generating many high-energy-electrons (active electrons). This is critical for catalysis activity, because the nitrogen fixation mechanism of metal atoms containing the process injecting the electrons into antibond of nitrogen. Since the metal atoms obtained additional active electrons when forming heterojunction, it is not surprised that the catalysis property of heterojunction is better than that of pure TiO_2. Furthermore, the defected interface leads to the variation of local atom's electronic properties, and some atoms with electronic properties benefiting catalysis become active sites. These phenomena will be further enhanced by OVs along with the interface, and OVs themselves act as active sites.

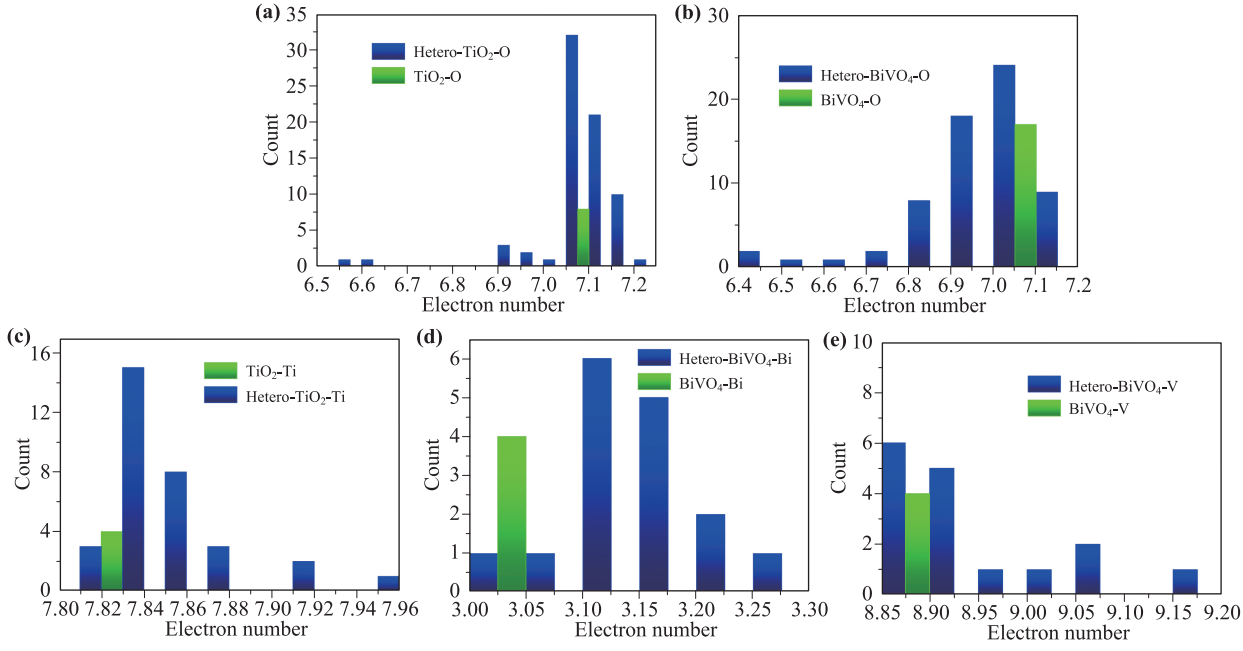


Fig. 11 The histogram of atom's charge of **(a)** O atoms in TiO_2, **(b)** O atoms in $BiVO_4$, **(c)** Ti atoms in TiO_2, **(d)** Bi atoms in $BiVO_4$ and **(e)** V atoms in $BiVO_4$. The green bins present the charge of single phase while the blue bins present the charge of phase in heterojunction. For the bins of same range, the green bin is always on the right.

5 Conclusion

In this paper, we developed a facile method to synthesize a $BiVO_4$/TNT catalyst which has a heterojunction interface with rich oxygen vacancies. Bismuth vanadate composite on TNT surface could form more oxygen vacancies and heterojunction structure between them, which not only provide a place for nitrogen adsorption, but also improve electron transfer ability and NRR catalytic activity, thus improving electrocatalytic nitrogen fixation performance. The synergistic effect of $BiVO_4$ and TNT can obviously decrease the protons transition distance and the over-potential of the nitrogen fixation reaction. The $BiVO_4$/TNT has a higher ammonia yield of 8.54 $\mu g \cdot h^{-1} \cdot cm^{-2}$ and higher FE of 7.70% at –0.8 V vs. RHE in 0.1 M Na_2SO_4 solution. This work could stimulate the rational designing of composite catalysts with heterojunction structure and rich oxygen vacancies.

Electronic supplementary material Electronic supplementary materials are available in the online version of this article at https://doi.org/10.1007/s11467-020-1067-8 and https://journal.hep.com.cn/fop/EN/10.1007/s11467-020-1067-8 are accessible for authorized users.

Acknowledgements This work was supported by the National Natural Science Foundation of China (Grant Nos. 51802126 and 52072152), the Jiangsu University Jinshan Professor Fund and Jiangsu Specially-Appointed Professor Fund, Open Fund from Guangxi Key Laboratory of Electrochemical Energy Materials. The authors also acknowledged the financial support by Guangdong Innovation Research Team for Higher Education (No. 2017KCXTD030) and High-level Talents Project of Dongguan University of Technology (No. KCYKYQD2017017).

References

1. P. Bhattacharya, D. E. Prokopchuk, and M. T. Mock, Exploring the role of pendant amines in transition metal complexes for the reduction of N_2 to hydrazine and ammonia, *Coord. Chem. Rev.* 334, 67 (2017)
2. J. R. Christianson, D. Zhu, R. J. Hamers, and J. R. Schmidt, Mechanism of N_2 reduction to NH_3 by aqueous solvated electrons, *J. Phys. Chem. B* 118(1), 195 (2014)
3. B. Qin, Y. Li, Q. Zhang, G. Yang, H. Liang, and F. Peng, Understanding of nitrogen fixation electro catalyzed by molybdenum–iron carbide through the experiment and theory, *Nano Energy* 68, 104374 (2020)
4. W. Zhao, S. Dou, K. Zhang, L. Wu, Q. Wang, D. Shang, and Q. Zhong, Promotion effect of S and N co-addition on the catalytic performance of V_2O_5/TiO_2 for NH_3-SCR of NO_x, *Chem. Eng. J.* 364, 401 (2019)
5. J. Zhao, Q. Ouyang, Q. Chen, and H. Lin, Simultaneous determination of amino acid nitrogen and total acid in soy sauce using near infrared spectroscopy combined with characteristic variables selection, *Food Sci. Technol. Int.* 19(4), 305 (2013)
6. B. Cui, J. Zhang, S. Liu, X. Liu, W. Xiang, L. Liu, H. Xin, M. J. Lefler, and S. Licht, Electrochemical synthesis of ammonia directly from N_2 and water over iron-based catalysts supported on activated carbon, *Green Chem.* 19(1), 298 (2017)
7. W. Qiu, X. Y. Xie, J. Qiu, W. H. Fang, R. Liang, X. Ren, X. Ji, G. Cui, A. M. Asiri, G. Cui, B. Tang, and X. Sun, High-performance artificial nitrogen fixation at ambient conditions using a metal-free electrocatalyst, *Nat. Commun.* 9(1), 3485 (2018)
8. Z. Cui, W. Du, C. Xiao, Q. Li, R. Sa, C. Sun, and Z. Ma, Enhancing hydrogen evolution of MoS_2 Basal planes by combining single-boron catalyst and compressive strain, *Front. Phys.* 15(6), 63502 (2020)
9. X. Chen, X. Zhao, Z. Kong, W. J. Ong, and N. Li, Unravelling the electrochemical mechanisms for nitrogen fixation on single transition metal atoms embedded in defective graphitic carbon nitride, *J. Mater. Chem. A* 6(44), 21941 (2018)
10. Z. X. Xu, H. Song, X. Q. Deng, Y. Y. Zhang, M. Xue-Qin, S. Q. Tong, Z. X. He, Q. Wang, Y. W. Shao, and X. Hu, Dewatering of sewage sludge via thermal hydrolysis with ammonia-treated Fenton iron sludge as skeleton material, *J. Hazard. Mater.* 379, 120810 (2019)
11. C. Liu, Q. Li, C. Wu, J. Zhang, Y. Jin, D. R. MacFarlane, and C. Sun, Single-boron catalysts for nitrogen reduction reaction, *J. Am. Chem. Soc.* 141(7), 2884 (2019)
12. Q. Li, C. Liu, S. Qiu, F. Zhou, L. He, X. Zhang, and C. Sun, Exploration of iron borides as electrochemical catalysts for the nitrogen reduction reaction, *J. Mater. Chem. A* 7(37), 21507 (2019)
13. Q. Li, S. Qiu, L. He, X. Zhang, and C. Sun, Impact of H-termination on the nitrogen reduction reaction of molybdenum carbide as an electrochemical catalyst, *Phys. Chem. Chem. Phys.* 20(36), 23338 (2018)
14. H. Cheng, L. X. Ding, G. F. Chen, L. Zhang, J. Xue, and H. Wang, Molybdenum carbide nanodots enable efficient electrocatalytic nitrogen fixation under ambient conditions, *Adv. Mater.* 30(46), 1803694 (2018)
15. X. Ren, J. Zhao, Q. Wei, Y. Ma, H. Guo, Q. Liu, Y. Wang, G. Cui, A. M. Asiri, B. Li, B. Tang, and X. Sun, High-performance N_2-to-NH_3 conversion electrocatalyzed by Mo_2C nanorod, *ACS Cent. Sci.* 5(1), 116 (2019)
16. Z. Sun, R. Huo, C. Choi, S. Hong, T. S. Wu, J. Qiu, C. Yan, Z. Han, Y. Liu, Y. L. Soo, and Y. Jung, Oxygen vacancy enables electrochemical N_2 fixation over WO_3 with tailored structure, *Nano Energy* 62, 869 (2019)
17. P. Chen, N. Zhang, S. Wang, T. Zhou, Y. Tong, C. Ao, W. Yan, L. Zhang, W. Chu, C. Wu, and Y. Xie, Interfacial engineering of cobalt sulfide/graphene hybrids for highly efficient ammonia electrosynthesis, *Proc. Natl. Acad. Sci. USA* 116(14), 6635 (2019)
18. M. Kitano, Y. Inoue, Y. Yamazaki, F. Hayashi, S. Kanbara, S. Matsuishi, T. Yokoyama, S. W. Kim, M. Hara, and H. Hosono, Ammonia synthesis using a stable electride as an electron donor and reversible hydrogen store, *Nat. Chem.* 4(11), 934 (2012)

19. F. Zhou, L. M. Azofra, M. Ali, M. Kar, A. N. Simonov, C. McDonnell-Worth, C. Sun, X. Zhang, and D. R. MacFarlane, Electro-synthesis of ammonia from nitrogen at ambient temperature and pressure in ionic liquids, *Energy Environ. Sci.* 10(12), 2516 (2017)
20. D. Wang, L. M. Azofra, M. Harb, L. Cavallo, X. Zhang, B. H. R. Suryanto, and D. R. MacFarlane, Energy-efficient nitrogen reduction to ammonia at low overpotential in aqueous electrolyte under ambient conditions, *Chem.Sus.Chem.* 11(19), 3416 (2018)
21. A. R. Singh, B. A. Rohr, J. A. Schwalbe, M. Cargnello, K. Chan, T. F. Jaramillo, I. Chorkendorff, and J. K. Nørskov, Electrochemical ammonia synthesis — The selectivity challenge, *ACS Catal.* 7(1), 706 (2017)
22. S. Z. Andersen, V. Čolić, S. Yang, J. A. Schwalbe, A. C. Nielander, J. M. McEnaney, K. Enemark-Rasmussen, J. G. Baker, A. R. Singh, B. A. Rohr, M. J. Statt, S. J. Blair, S. Mezzavilla, J. Kibsgaard, P. C. K. Vesborg, M. Cargnello, S. F. Bent, T. F. Jaramillo, I. E. L. Stephens, J. K. Nørskov, and I. Chorkendorff, A rigorous electrochemical ammonia synthesis protocol with quantitative isotope measurements, *Nature* 570(7762), 504 (2019)
23. J. Kibsgaard, J. K. Nørskov, and I. Chorkendorff, The Difficulty of Proving Electrochemical Ammonia Synthesis, *ACS Energy Lett.* 4(12), 2986 (2019)
24. T. Chen, S. Liu, H. Ying, Z. Li, and J. Hao, Reactive ionic liquid enables the construction of 3D Rh particles with nanowire subunits for electrocatalytic nitrogen reduction, *Chem. Asian J.* 15(7), 1081 (2020)
25. H. Xie, Q. Geng, X. Zhu, Y. Luo, L. Chang, X. Niu, X. Shi, A. M. Asiri, S. Gao, Z. Wang, and X. Sun, PdP_2 nanoparticles-reduced graphene oxide for electrocatalytic N_2 conversion to NH_3 under ambient conditions, *J. Mater. Chem. A* 7(43), 24760 (2019)
26. Z. Zhang, K. Yao, L. Cong, Z. Yu, L. Qu, and W. Huang, Facile synthesis of a Ru-dispersed N-doped carbon framework catalyst for electrochemical nitrogen reduction, *Catal. Sci. Technol.* 10(5), 1336 (2020)
27. X. Zhao, Z. Yang, A. V. Kuklin, G. V. Baryshnikov, H. Ågren, W. Wang, X. Zhou, and H. Zhang, Potassium ions promote electrochemical nitrogen reduction on nano-Au catalysts triggered by bifunctional boron supramolecular assembly, *J. Mater. Chem. A* 8(26), 13086 (2020)
28. D. Deng, K. S. Novoselov, Q. Fu, N. Zheng, Z. Tian, and X. Bao, Catalysis with two-dimensional materials and their heterostructures, *Nat. Nanotechnol.* 11(3), 218 (2016)
29. D. Gao, Y. Zhang, Z. Zhou, F. Cai, X. Zhao, W. Huang, Y. Li, J. Zhu, P. Liu, F. Yang, G. Wang, and X. Bao, Enhancing CO_2 electroreduction with the metal–oxide interface, *J. Am. Chem. Soc.* 139(16), 5652 (2017)
30. Y. Guo, J. Zou, X. Shi, P. Rukundo, and Z. Wang, A Ni/CeO_2–CDC-SiC catalyst with improved Coke resistance in CO_2 reforming of methane, *ACS Sustain. Chem. & Eng.* 5(3), 2330 (2017)
31. S. Xie, Y. Liu, J. Deng, J. Yang, X. Zhao, Z. Han, K. Zhang, Y. Lu, F. Liu, and H. Dai, Carbon monoxide oxidation over rGO-mediated gold/cobalt oxide catalysts with strong metal–support interaction, *ACS Appl. Mater. Interfaces* 12(28), 31467 (2020)
32. H. C. Song, G. R. Lee, K. Jeon, H. Lee, S. W. Lee, Y. S. Jung, and J. Y. Park, Engineering nanoscale interfaces of metal/oxide nanowires to control catalytic activity, *ACS Nano* 14(7), 8335 (2020)
33. J. Lv, S. Wu, Z. Tian, Y. Ye, J. Liu, and C. Liang, Construction of PdO–Pd interfaces assisted by laser irradiation for enhanced electrocatalytic N_2 reduction reaction, *J. Mater. Chem. A* 7(20), 12627 (2019)
34. B. Xu, L. Xia, F. Zhou, R. Zhao, H. Chen, T. Wang, Q. Zhou, Q. Liu, G. Cui, X. Xiong, F. Gong, and X. Sun, Enhancing Electrocatalytic, N_2 reduction to NH_3 by CeO_2 nanorod with oxygen vacancies, *ACS Sustain. Chem. & Eng.* 7(3), 2889 (2019)
35. W. Fu, P. Zhuang, M. OliverLam Chee, P. Dong, M. Ye, and J. Shen, Oxygen vacancies in Ta_2O_5 nanorods for highly efficient electrocatalytic N_2 reduction to NH_3 under ambient conditions, *ACS Sustain. Chem. & Eng.* 7(10), 9622 (2019)
36. Y. Tong, H. Guo, D. Liu, X. Yan, P. Su, J. Liang, S. Zhou, J. Liu, G. Q. Lu, and S. X. Dou, Vacancy engineering of iron-doped $W_{18}O_{49}$ nanoreactors for low-barrier electrochemical nitrogen reduction, *Angew. Chem. Int. Ed.* 59(19), 7356 (2020)
37. T. Wu, X. Zhu, Z. Xing, S. Mou, C. Li, Y. Qiao, Q. Liu, Y. Luo, X. Shi, Y. Zhang, and X. Sun, Greatly improving electrochemical N_2 reduction over TiO_2 nanoparticles by iron doping, *Angew. Chem. Int. Ed.* 58(51), 18449 (2019)
38. T. Wu, W. Kong, Y. Zhang, Z. Xing, J. Zhao, T. Wang, X. Shi, Y. Luo, and X. Sun, Greatly enhanced electrocatalytic N_2 reduction on TiO_2 via V doping, *Small Methods* 3(11), 1900356 (2019)
39. S. Cheng, Y. J. Gao, Y. L. Yan, X. Gao, S. H. Zhang, G. L. Zhuang, S. W. Deng, Z. Z. Wei, X. Zhong, and J. G. Wang, Oxygen vacancy enhancing mechanism of nitrogen reduction reaction property in Ru/TiO_2, *J. Energ. Chem.* 39, 144 (2019)
40. Z. Han, C. Choi, S. Hong, T. S. Wu, Y. L. Soo, Y. Jung, J. Qiu, and Z. Sun, Activated TiO_2 with tuned vacancy for efficient electrochemical nitrogen reduction, *Appl. Catal. B* 257, 117896 (2019)
41. B. Li, X. Zhu, J. Wang, R. Xing, Q. Liu, X. Shi, Y. Luo, S. Liu, X. Niu, and X. Sun, Ti^{3+} self-doped TiO_{2-x} nanowires for efficient electrocatalytic N_2 reduction to NH_3, *Chem. Commun. (Camb.)* 56(7), 1074 (2020)
42. Y. T. Liu, X. Chen, J. Yu, and B. Ding, Carbon-nanoplated CoS@TiO_2 nanofibrous membrane: An interface-engineered heterojunction for high-efficiency electrocatalytic nitrogen reduction, *Angew. Chem. Int. Ed.* 58(52), 18903 (2019)
43. M. M. Shi, D. Bao, B. R. Wulan, Y. H. Li, Y. F. Zhang, J. M. Yan, and Q. Jiang, Au sub-nanoclusters on TiO_2 toward highly efficient and selective electrocatalyst for N_2 conversion to NH_3 at ambient conditions, *Adv. Mater.* 29(17), 1606550 (2017)
44. J. Zhang, Y. Tian, T. Zhang, Z. Li, X. She, Y. Wu, Y. Wang, and J. Wu, Confinement of intermediates in blue TiO_2 nanotube arrays boosts reaction rate of nitrogen electrocatalysis, *Chem. Cat. Chem.* 12(10), 2760 (2020)

45. P. Zhao, L. Zhang, J. Song, S. Wen, and Z. Cheng, Phosphorus cation substitution in TiO_2 nanorods toward enhanced N_2 electroreduction, *Appl. Surf. Sci.* 523, 146517 (2020)
46. Q. Hao, C. Liu, G. Jia, Y. Wang, H. Arandiyan, W. Wei, and B. J. Ni, Catalytic reduction of nitrogen to produce ammonia by bismuth-based catalysts: State of the art and future prospects, *Mater. Horiz.* 7(4), 1014 (2020)
47. L. Li, C. Tang, B. Xia, H. Jin, Y. Zheng, and S. Z. Qiao, Two-dimensional mosaic bismuth nanosheets for highly selective ambient electrocatalytic nitrogen reduction, *ACS Catal.* 9(4), 2902 (2019)
48. J. M. Wu, Y. Chen, L. Pan, P. Wang, Y. Cui, D. Kong, L. Wang, X. Zhang, and J. J. Zou, Multi-layer monoclinic $BiVO_4$ with oxygen vacancies and V^{4+} species for highly efficient visible-light photoelectrochemical applications, *Appl. Catal. B* 221, 187 (2018)
49. J. X. Yao, D. Bao, Q. Zhang, M. M. Shi, Y. Wang, R. Gao, J. M. Yan, and Q. Jiang, Tailoring oxygen vacancies of $BiVO_4$ toward highly efficient noble-metal-free electrocatalyst for artificial N_2 fixation under ambient conditions, *Small Methods* 3(6), 1800333 (2019)
50. C. Ling, Y. Zhang, Q. Li, X. Bai, L. Shi, and J. Wang, New mechanism for N_2 reduction: The essential role of surface hydrogenation, *J. Am. Chem. Soc.* 141(45), 18264 (2019)